Ghosting Reflection Compensation for Multispectral High Dynamic Range Imaging

Johannes Brauers and Til Aach

Institute of Imaging & Computer Vision, RWTH Aachen University, Templergraben 55, D-52056 Aachen, Germany

Abstract

A compact overall design of a multispectral camera can be achieved by placing the bandpass filters between the lens and sensor. However, internal reflections between the sensor (or IR cut filter) and the optical filters may lead to weak duplicate images which impair the image quality. The duplicates called ghosting are especially noticeable near bright image regions and interfere with the surrounding image content. When using combined high dynamic range (HDR) and multispectral imaging, the increased dynamic range is of reduced value due to the ghosting.

In the current paper, we model the ghosting effect and present a calibration setup for the characterization of the ghosting, which utilizes a backlit film calibration pattern. We perform HDR imaging to acquire the vast dynamic range of the backlit scene. Our calibration algorithm then estimates the model parameters and allows a compensation of the ghosting. As long as the lens parameters are not changed, the calibration may be used for all subsequent images. We give detailed results for the calibration and the effect of the compensation.

Introduction

Figure 1. *Seven channel multispectral camera with its internal configuration sketched.*

A widely-used multispectral imaging technique utilizes optical bandpass filters to divide the visible light spectrum into several passbands. The concept has once been patented in [1]. Several uses of the technique are reported in [2, 3, 4, 5, 6] – to name only a few. In a special variant described in [7] the optical filters are placed between the sensor and the lens. This kind of camera exhibits three main advantages compared to a camera system where the filter wheel is placed between the lens and the object: First, the small required filter sizes allow a compact and portable camera design. Second, the lens rather than the filter wheel is the outmost optical element. Therefore, all damageable movable parts are inside the multispectral camera. Third, the lens can be easily exchanged like in a consumer single lens reflex system. For instance, a wide angle lens could be easily exchanged by a telephoto lens without changing the camera setup. We used this camera type to acquire multispectral images with flash light sources [8].

However, the placement of the optical filters in a critical part of the imaging system – namely between lens and CCD – has also its downside: Depending on the quality of the filter coating, camera internal reflections may occur. The usual lens-internal reflections are thus intensified by reflections between the lens exit surface and the optical filter. This causes a low-frequency, strongly blurred *stray light* or *glare*. For reflections occurring between the optical bandpass filter and the sensor, the resulting distortions in the image are rather sharp or focused and are called *ghosting*. In this paper, we consider the latter case. The ghosting may cause serious color distortions and thus compromise high fidelity color reproduction. For example, in the left part of Fig. 7 the ghosting shows up as colored crosses.

Our algorithms are derived for a multispectral camera system where the filters are placed between sensor and lens. There might be other camera types using this specific system setup – e.g., a LCTF (light crystal tunable filter) camera [9] – where the algorithms are also applicable. However, we were only able to test the algorithms with our seven channel filter wheel camera.

To clarify the terminology, let us briefly mention that in the context of HDR imaging, the notion of ghosting compensation has been used by some authors in a different context: Khan et al. in [10] discuss the inconsistencies which occur in successively acquired images with varying exposures for HDR imaging when the scene is moving, e.g., because of walking people. These inconsistencies manifest themselves as ghost-like replicas of the moving objects which do not originate from a multispectral acquisition, which is the focus of this contribution.

A method to reduce stray light in multispectral cameras is described by Helling in [11]. While he discusses low-frequency stray light with a large spread over the image, we consider a local, rather focused effect called ghosting. Both methods complement each other, but differ significantly in their calibration and compensation method since they have been developed for different applications.

An approach for the reduction of "veiling glare" (stray light) in RGB cameras is presented in [12]: The authors place a special grid hole mask at different locations between the camera and the scene for each image they acquire. This enables them to characterize the low-frequency glare in the image. We find the placement of an additional mask not suitable for our application and focus on ghosting instead of glare.

A more generic model than the one used here is provided

in [13], where the authors assume a variable point spread function (PSF) for each image position. However, the estimation of such PSFs is not described. Their results are based on a simulation with a known PSF.

In [14], we have described an early version of our compensation method, which covers the compensation of a single passband solely. Here, we use an improved calibration setup and apply our algorithm for all spectral passbands. This enables us for the first time to evaluate the results on seven-channel multispectral and RGB images. We are thus able to provide much more detailed results.

We start with a description of our model and the measurement setup. In the following section, we present our calibration algorithm which estimates the ghosting model parameters from images acquired with the setup in the previous section. We then describe our results in detail and conclude with a discussion.

Theory and Measurement Setup

The formation of ghosting in a multispectral camera with filters between lens and sensor is illustrated in Fig. 2: Incident light rays originating from the lens (not shown) impinge on the optical filter at position ①. As discussed in [15], it is practically infeasible to align the optical bandpass filters in a perfectly coplanar manner and perfectly parallel to the sensor. We therefore need to consider an individual tilt angle for each optical filter in the filter wheel. In this particular example, the ray is perpendicular to the normal vector of the filter and therefore not refracted. We discussed other cases in [15]. The ray leaves the optical filter at position ② and arrives at the sensor at ③, where the original image is produced. Because of the reflectivity of the sensor (or its prepended IR cut filter), the ray is reflected partly and impinges at the optical filter at position ④. Depending on the quality of the surface coating of the filter, the ray is once more partly reflected and appears at the position ⑤ on the sensor. Here, a weak duplicate image we call *ghosting* is produced.

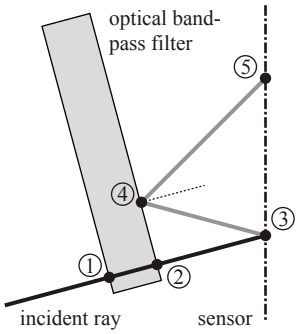

Figure 2. *Formation of ghosting: incident rays ① are reflected at the sensor ③ (or its IR cut filter), the tilted bandpass filter ④ and appear as a duplicate image (ghosting) on the sensor at a different position ⑤.*

The model allows us to derive three conclusions: Since the surfaces are coated, the reflections of the rays are rather weak – we assume a certain reflection factor r, which describes the gray level relation between original and ghosting image. Second, the ghosting ray (and also image) appears at a different position ⑤ than the original image ③, because we assume that the filter is slightly tilted. We have shown in [14] that the underlying geometrical relation between original and ghosting image is a projective transformation. Even when the filters and the sensor would be aligned in a perfectly coplanar manner, the other conclusions given here remain valid. Third, due to the increased path length of the ghosting (additional sections ③-⑤), the ghosting image is not focused any more. Figs. 6 and 7 show examples of original symbols and their ghosting duplicates; the figure is discussed in the results section.

We model the ghosting effect mathematically by

$$g(x,y) = f(x,y) + rf(x',y') * h_\sigma(x,y), \tag{1}$$

where $f(x,y)$ is the original image, $g(x,y)$ is the tampered image including the ghosting and r is the reflection factor described above. The Gaussian shaped point spread function $h_\sigma(x,y)$ with the standard deviation σ is convolved with a geometrically transformed version of the original image $f(x',y')$. The geometric transformation is given by

$$\begin{pmatrix} u & v & w \end{pmatrix}^T = \mathbf{M} \begin{pmatrix} x & y & 1 \end{pmatrix}^T \tag{2}$$

and

$$x' = \frac{u}{w} \qquad y' = \frac{v}{w}, \tag{3}$$

where the original coordinates are given by x, y, the transformed ones by x', y' and the transformation matrix itself by $\mathbf{M} = \mathbb{R}^{3\times 3}$. Details on the projective transformations may be found in the computer vision literature [16].

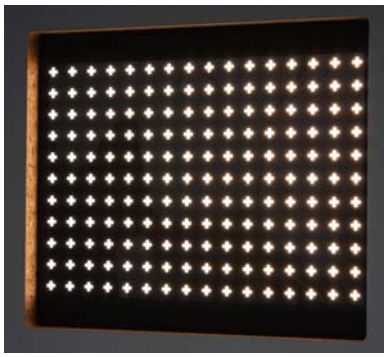

Figure 3. *Our calibration setup: A 297 mm×210 mm film with cross symbols on it is back-illuminated by a halogen bulb and diffusers.*

Because the ghosting is approximately one hundred times weaker than the original image, we have developed a special calibration setup for the characterization of the ghosting and estimation of the model parameters (see Fig. 3): A film with cross symbols is back-illuminated with a 1600 watt halogen bulb. To ensure a homogeneous illumination of this partly transparent calibration target, we placed several diffusers between the target and the lamp. In the black areas, the target is practically opaque. Use of this target facilitates quantification of ghosting considerably from its appearances in the originally black target areas.

Calibration Algorithm

The images of the calibration target shown in Fig. 6 serve as input for our calibration algorithm. They show the original cross

symbols and their corresponding weak ghosting duplicates. The calibration has to be done for each spectral passband separately. Our goal is to estimate three parameters:

- The gray level relation between original and ghosting image, i.e., the joint reflection factor r.
- The projection between original and ghosting, i.e., a displacement vector $(\Delta x, \Delta y)$ or transformation matrix.
- The blurring of the ghosting image compared to the original, which we model using a Gaussian shaped point spread function (PSF) with a standard deviation σ.

Our calibration algorithm accomplishes the estimation of the above parameters and is shown in Fig. 4: Because of our specific calibration target, it is – in most cases – possible to estimate a gray level threshold which separates the ghosting symbols from the original ones. By thresholding the image, we obtain a mask, which is slightly enlarged using morphological dilation. The dilation is applied to ensure that the bright original symbols are completely enclosed in the mask. The output of the first major step (shown in the top horizontal box on the left in Fig. 4) are two images: the first shows only the original symbols, the second one only the ghosting duplicates.

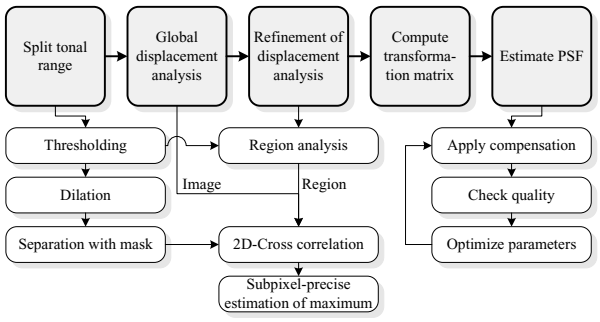

Figure 4. *Block diagram of the ghosting compensation algorithm. The shaded blocks in the top row show the succession of major processing steps, with more block-internal details given below each block.*

After that, a two-dimensional cross correlation is performed to determine the *global displacement* between the originals and their ghosting counterparts. The displacement is due to the slight tilt of the optical filters as shown in Fig. 2. In the next step (*refinement*), the displacement is refined using a region-based analysis: Cross correlation is performed for each symbol separately. The result of this step is a displacement vector field, where each vector represents the displacement between each symbol and its ghosting duplicate. From these vectors, we determine a *transformation matrix* which models the geometric relations between original and ghosting symbols. The matrix allows us to estimate the displacement for each pixel in our original image.

So far, only the geometric displacement between original and ghosting symbols has been estimated. The subsequent estimation of the blur and the reflection factor is carried out in an iterative optimization loop. Therefore, the compensated image, i.e., the estimation of the original image

$$\hat{f}(x,y) = g(x,y) - r f(x',y') * h_\sigma(x,y)\,, \qquad (4)$$

which is derived from Eq. (1) to (3), is considered. The parameters of this term are found by minimizing the variance of $\hat{f}(x,y)$ in an area $m(x,y)$ which excludes the original symbols. In other words, the variance is estimated in the dark areas surrounding the original symbols (see Fig. 6). These areas are brightened by the ghosting symbols in the acquired calibration images but should be homogeneous (low variance) after the compensation. We estimate the parameters with

$$(r,\sigma) = \arg\min_{r,\sigma} \|m(x,y)\hat{f}(x,y) - \|m(x,y)\hat{f}(x,y)\|\,\|^2\,, \qquad (5)$$

using the Nelder and Mead simplex method [17] implemented in Matlab®'s `fminsearch` function.

The compensation itself is done by applying the steps implicitly described by Eq. (4): First, geometrically transform the image using the transformation matrix estimated above. Second, blur the resulting image using a Gaussian shaped PSF using the standard deviation σ, which has been estimated in the optimization process. Third, reduce the amplitude of the image by the reflection factor r, which also has been estimated above. Forth, subtract the synthetically generated ghosting image from the original image – the result is the compensated image.

Results

To validate our algorithm, we use the multispectral camera shown in Fig. 1: Its internal gray scale camera provides a resolution of 1280×960 pixel at a bit depth of 8 bit. A reduction of noise is achieved by averaging multiple images or performing multispectral HDR imaging as described in [18]. The internal camera filter wheel is equipped with seven optical bandpass filters from Andover Corporation in the range from 400 nm to 700 nm with a bandwidth of 40 nm each and a wavelength increment of 50 nm. The lens is a Nikkor AF-S DX 18-70 mm.

Figure 5. *Exposure series of acquired images for high dynamic range imaging (500 nm band). It can be seen that the original cross symbol is acquired correctly as well as its weak ghosting duplicate.*

Since the calibration images span a vast dynamic range, we performed the acquisition with multispectral HDR imaging [18]: Towards this end, we acquired each spectral channel with ten different exposure times as shown in Fig. 5. In this way, we are able to acquire both the *original* cross symbols and their ghosting duplicates correctly. Each one of the ten consecutive exposures for one spectral passband is taken $\sqrt{2}$ times longer than the preceding one. All in all, we therefore acquire images with exposure times from t to $2^{10/2}t = 32t$, where t is the initial exposure time. Saturated areas from specific exposures are not included in the final multispectral image.

We acquire HDR calibration images for all spectral passbands (see crops in Fig. 6). Because each spectral bandpass filter is placed in a slightly different pose in the computer-controlled filter wheel, the reflection as shown in Fig. 2 varies for each filter position. Therefore, also the ghosting crosses appear at different positions relative to the original symbols. From the calibration images we derive the ghosting parameters shown in Tab. 1 with

Figure 6. *Series of calibration image crops for all spectral channels (from 400 nm to 700 nm. The parameters in Table 1 are computed from these calibration images.*

our algorithm described above. The strength of the blurring is related to the parameter σ: The second to topmost calibration image is the sharpest one ($\sigma = 0.47$), whereas the last but one calibration image is the most blurry one ($\sigma = 7$). The reflection factor r varies slightly, but we can approximately state that the ghosting duplicate is one hundred times weaker than the original image. This confirms our requirement of HDR imaging to correctly characterize the ghosting. However, once the parameters have been *estimated* using HDR imaging, the *compensation* can also be applied to images with a normal dynamic range. The displacements given in Tab. 1 describe the main geometric distortions between the original and ghosting images; we omitted the full projection matrices $\mathbf{M}$ described in Eq. (2).

	σ	r	Δx [Pixel]	Δy [Pixel]
400 nm	2.27	0.02	7.26	23.01
450 nm	0.47	0.01	6.74	26.22
500 nm	2.18	0.01	13.46	24.15
550 nm	2.66	0.01	27.05	24.45
600 nm	2.77	0.02	-9.66	-22.69
650 nm	7.00	0.01	0.46	6.44
700 nm	2.48	0.02	17.17	-2.96

Table 1. Estimated parameters from the ghosting analysis for all spectral passbands.

The sRGB images in Fig. 7 have been computed from the seven grayscale passband images [18]: A spectral vector is computed for each pixel, then transformed to XYZ color space and finally transformed to the sRGB color space. The images are calculated for the D50 illuminant using the CIE 1931 observer. The left image has not been compensated for ghosting and thus shows colored cross symbols in the background which are caused by the ghosting effect described above. The right image has been compensated and the ghosting vanishes. Both images have been brightened to highlight the effect.

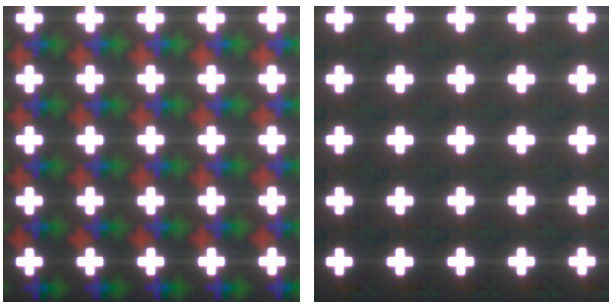

Figure 7. *Original (left) and ghosting compensated calibration images (right), both approx. brightened 8-fold. The colored ghosting duplicates in the left image are caused by the different spectral transmittance curves of the optical bandpass filters.*

The images in Fig. 8 have been produced in the same manner as the ones in Fig. 7 and show a small part of the ColorChecker SG. While the ghosting is hardly visible in the lower images, which have not been brightened, it clearly appears in the images above. Especially the bright color patches produce a relatively strong ghosting (see patch A10, e.g.).

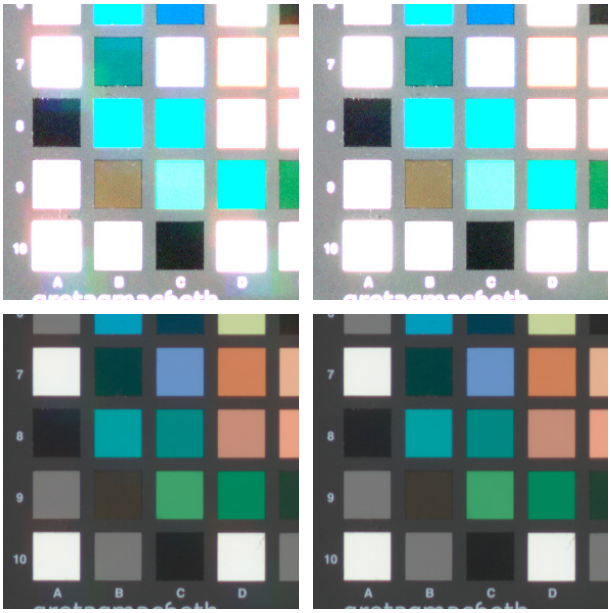

Figure 8. *Original (left) and ghosting compensated images (right). The upper image row is brightened five-fold. Colored duplicates of the original passband images are clearly visible next to bright color patches in the left image.*

We also performed colorimetric analysis in Fig. 9: The color value of each area marked with red rectangles is averaged and compared to a reference value measured with a spectral photometer. This comparison is done for both the original and the compensated image. The numbers in the figure denote the difference between the original and compensated image. Especially in the black patch, where the ghosting produced by the upper white patch influences the black patch, the color reproduction can be enhanced drastically (improvement of $+2.66\ \Delta E_{00}$). In some areas, there is also a slight degradation of the color accuracy caused by a slight overcompensation and imperfections of the Gaussian model. However, these degradations are always 5 to 10 times lower than the achieved improvements, and thus have only a minor influence on the enhanced result.

Conclusions and Discussion

We have shown promising results for the compensation of ghosting in multispectral filter wheel cameras. A detailed report of our practical imaging experiments includes estimated calibration parameters, a colorimetric analysis and descriptive images. Especially dark regions, which are disturbed by nearby bright spots benefit from our method.

The compensation is based on a theoretical model for the ghosting, the parameter estimation of which is *not* ill-posed, but instead can be estimated by our software algorithm. We presented a special calibration setup being suitable for the characterization

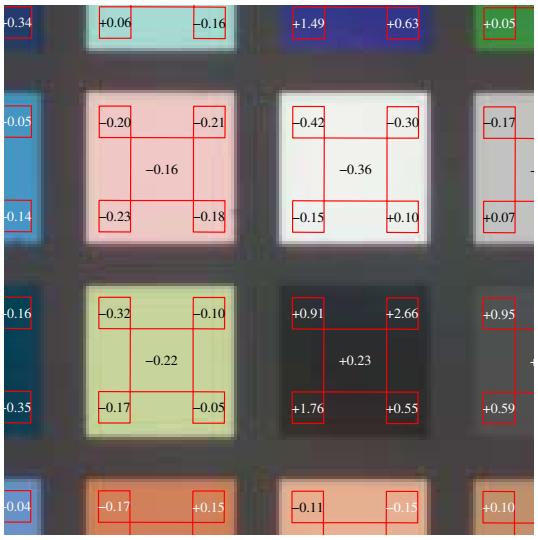

Figure 9. *Detailed color error analysis for some ColorChecker patches: positive ΔE_{00}-numbers indicate improvements due to ghosting compensation; especially the border regions of the dark patch benefit from the compensation.*

of the weak ghosting effect, which is approximately one hundred times weaker than the original image, but may still induce color distortions. Multispectral HDR imaging provides the facilities to cope with the extreme dynamic range of the calibration scene. However, the compensation itself can also be applied to an image with normal dynamic range. The dynamic range of the image itself is not modified by our algorithm.

As yet, it is necessary to adjust the model parameters for the ghosting manually for cases in which the original calibration symbol and its ghosting duplicate overlap to a certain extent. In the future it might be possible to develop a method to automatically estimate the ghosting parameters even in this case. Because the ghosting is very weak and noisy, we chose a Gaussian shaped point spread function to model the blurring caused by the defocus of the ghosting. However, it would be more appropriate to use a custom-shaped and spatially varying PSF like in [19]. Although ghosting and stray light [11] seem to be very similar, their characterization is actually different. Nevertheless, it might be possible to derive a combined model for both phenomena.

Acknowledgments

The authors are grateful to B. Hill and S. Helling for many fruitful discussions. They also acknowledge gratefully funding by the German Research Foundation (DFG, grant AA5/2-1).

References

[1] B. Hill and F. W. Vorhagen, "Multispectral image pick-up system," 1991. U.S.Pat. 5,319,472, German Patent P 41 19 489.6.

[2] M. Yamaguchi, H. Haneishi, and N. Ohyama, "Beyond Red-Green-Blue (RGB): Spectrum-based color imaging technology," *Journal of Imaging Science and Technology* **52**, pp. 010201–1–010201–15, Jan 2008.

[3] S. Tominaga, "Spectral imaging by a multi-channel camera," *Journal of Electronic Imaging* **8**, pp. 332–341, Oct 1999.

[4] P. D. Burns and R. S. Berns, "Analysis multispectral image capture," in *IS&T Color Imaging Conference*, **4**, pp. 19–22, (Springfield, VA, USA), 1996.

[5] A. Mansouri, F. S. Marzani, J. Y. Hardeberg, and P. Gouton, "Optical calibration of a multispectral imaging system based on interference filters," *SPIE Optical Engineering* **44**, pp. 027004.1–027004.12, Feb 2005.

[6] H. Haneishi, T. Iwanami, T. Honma, N. Tsumura, and Y. Miyake, "Goniospectral imaging of three-dimensional objects," *Journal of Imaging Science and Technology* **45**(5), pp. 451–456, 2001.

[7] S. Helling, E. Seidel, and W. Biehlig, "Algorithms for spectral color stimulus reconstruction with a seven-channel multispectral camera," in *IS&Ts Proc. 2nd European Conference on Color in Graphics, Imaging and Vision CGIV 2004*, **2**, pp. 254–258, (Aachen, Germany), Apr 2004.

[8] J. Brauers, S. Helling, and T. Aach, "Multispectral image acquisition with flash light sources," *Journal of Imaging Science and Technology* **53**(3), pp. 031103–1–031103–10, 2009.

[9] "Cambridge Research & Instrumentation, Inc.."

[10] E. Khan, A. Akyuz, and E. Reinhard, "Ghost removal in high dynamic range images," in *IEEE International Conference on Image Processing*, pp. 2005–2008, (Atlanta, Georgia, USA), Oct 2006.

[11] S. Helling, "Improvement of multispectral image capture by compensating for stray light," in *Proc. 3nd European Conference on Color in Graphics, Imaging and Vision CGIV 2006*, pp. 458–462, (Leeds, UK), June 2006.

[12] E.-V. Talvala, A. Adams, M. Horowitz, and M. Levoy, "Veiling glare in high dynamic range imaging," in *ACM SIGGRAPH 2007 papers*, p. 37, ACM, (New York, NY, USA), 2007.

[13] P. A. Jansson and R. P. Breault, "Correcting color-measurement error caused by stray light in image scanners," in *IS&T/SID Sixth Color Imaging Conference: Color Science, Systems and Applications*, **6**, pp. 69–73, (Scottsdale, Arizona, USA), Nov 1998.

[14] J. Brauers and T. Aach, "Modeling and compensation of ghosting in multispectral filter wheel cameras," in *IEEE Southwest Symposium on Image Analysis and Interpretation*, pp. 85–88, (Santa Fe, New Mexico, USA), Mar 2008.

[15] J. Brauers, N. Schulte, and T. Aach, "Multispectral filter-wheel cameras: Geometric distortion model and compensation algorithms," *IEEE Transactions on Image Processing* **17**, pp. 2368–2380, Dec 2008.

[16] R. I. Hartley and A. Zisserman, *Multiple View Geometry in Computer Vision*, Cambridge University Press, ISBN: 0521540518, second ed., 2004.

[17] J. Nelder and R. Mead, "A simplex method for function minimization," *Computer Journal* **7**, pp. 308–313, 1965.

[18] J. Brauers, N. Schulte, A. A. Bell, and T. Aach, "Multispectral high dynamic range imaging," in *IS&T/SPIE Electronic Imaging*, **6807**, (San Jose, California, USA), Jan 2008.

[19] J. Brauers and T. Aach, "Longitudinal aberrations caused by optical filters and their compensation in multispectral imaging," in *IEEE International Conference on Image Processing (ICIP2008)*, pp. 525–528 (CD–ROM), IEEE, (San Diego, CA, USA), Oct 2008.